*Journal of Fluids and Structures* (1999) **13,** 269–287
Article No.: jfls.1998.0196 available online at http://www.idealibrary.com on IDEAL

# ACTIVE NOZZLE CONTROL AND INTEGRATED DESIGN OPTIMIZATION OF A BEAM SUBJECT TO FLUID-DYNAMIC FORCES

D. BORGLUND

*Department of Aeronautics, Royal Institute of Technology SE-100 44 Stockholm, Sweden*

(Received 23 March 1998 and in revised form 22 July 1998)

Active nozzle control is used to improve the stability of a beam subject to forces induced by fluid flow through attached pipes. The control system has a significant effect on the structural stability, making both flutter and divergence type of instabilities possible. The stability analysis is carried out using a state-variable approach based on a finite element formulation of the structural dynamics. The simultaneous design of the control system and the beam shape minimizing structural mass is performed using numerical optimization. The inclusion of the control system in the optimization gives a considerable reduction of the structural mass but results in an optimal design which is very sensitive to imperfections. Using a simple model of the control system uncertainties, a more robust design is obtained by solving a modified optimization problem. Throughout the study, the theoretical findings are verified by experiments.


## 1. INTRODUCTION

IN RECENT YEARS, there has been significant interest in the use of active control to stabilize flexible structures. This paper deals with the control and optimal design of a flexible structure subject to nonconservative fluid-dynamic forces. While the system investigated is somewhat simplistic, an important aeronautical application within this class of problems is an aircraft wing subject to aerodynamic loads. The optimal design of an aircraft wing typically involves minimization of structural mass subject to constraints on structural stability (Kuttenkeuler & Ringertz 1998a), while active control typically involves flutter suppression (Zhou *et al*. 1995). An appealing concept to be demonstrated in this paper is to use the increased stability from an active control system to further reduce the structural mass. Naturally, this leads to a formulation of the optimization problem where the structural mass is minimized using both structural dimensions and control system parameters as design variables.

A flexible pipe conveying fluid has been used as a model problem for structures subject to nonconservative forces in many studies. An extensive review on this subject is given by Paidoussis & Li (1993). In particular, the problem of optimal design of pipes conveying fluid has been studied by Langthjem (1996), Tanaka *et al*. (1993) and Borglund (1998). Examples of work on active control of the same mechanical system are Yau *et al*. (1995) and Chen & Jendrzejczyk (1985).

The purpose of the present paper is to illustrate integrated design optimization and investigate what impact the inclusion of a control system may have on the properties of the optimal design. The modified pipe-flow system investigated in Borglund (1998) serves as a model problem. A linear state-variable formulation of the control theory is used for two main reasons. First, the stability analysis is then identical to the case without control.

0889–9746/99/020269 + 19 $30.00 

Second, using the state-variable feedback gains as design variables provides simple calculations of the stability constraint function derivatives used in the optimization. Experimental verification of predicted design improvements and properties of the optimal design is emphasized.

## 2. THE MODEL PROBLEM

A schematic layout of the system is shown in Figure 1. A thin and slender beam is subject to fluid-dynamic forces due to water flow in two attached circular tubes, aligned symmetrically on each side. A cantilevered configuration hanging vertically downward is considered. It is well known that a configuration such as this may become unstable in flutter at some critical flow speed (Borglund 1998).

In a previous study (Borglund 1998), the beam-tube structure was found to be accurately modelled by a flexible beam with centred flow, thus having the same dynamics as a cantilevered pipe conveying fluid. In this study, the system is extended by including a nozzle control system, clamped to the beam-tube structure at the downstream end. By properly controlling the nozzles in parallel, the applied loads at the beam tip may stabilize the system and increase the critical speed for a fixed design of the beam. Using the centered flow approximation, the nozzle control system is considered as composed of two rigid pipes of finite length. The first of these pipes represent the actual control system which is clamped to the beam. The second represents the nozzles, modelled as a single pipe abruptly deflecting the centred flow at the nozzle inlet.

### 2.1. Equation of Motion

The beam is modelled using a viscoelastic Kelvin–Voigt material model (Langthjem 1996) with density $\rho_b$, Young's modulus $E_b$ and dynamic viscosity coefficient $E_b^*$. The beam

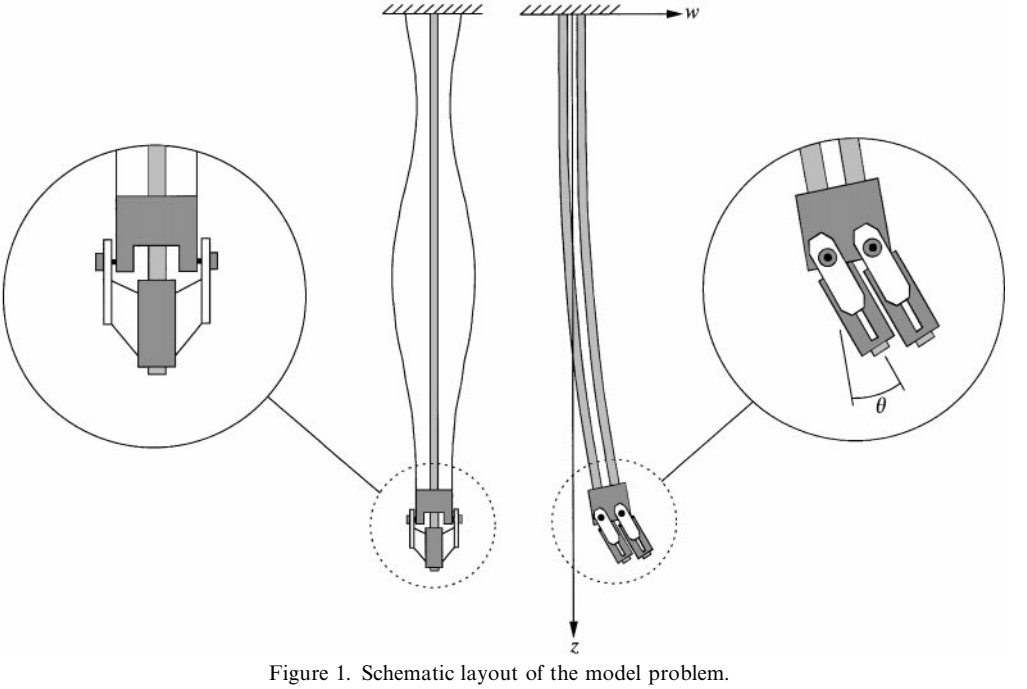


Figure 1. Schematic layout of the model problem.

geometry is given by the length $l$, width $h(z)$, and constant thickness $d$, giving an area-moment of inertia $I_b(z)$ and mass per unit length $m_b(z)$. Using the same material model, the tubes have the corresponding properties $\rho_t$, $E_t$ and $E_t^*$, but have a fixed geometry with total area-moment of inertia (with respect to the beam center axis) $I_t$ and total mass per unit length $m_t$. The tubes convey a fluid with total mass per unit length $m_f$ and flow speed $u$.

The control system has length $l_c$ and total mass $M_c$, including the mass $M_{fc}$ of the enclosed fluid. The distance from the beam end to the center of mass of the control system is denoted $a_c$, and the corresponding distance for the enclosed fluid is $a_{fc} = l_c/2$ (see Figure 12 in the appendix). The corresponding quantities for the nozzle are $l_n$, $M_n$, $M_{fn}$, $a_n$ and $a_{fn} = l_n/2$, where distances are measured from the nozzle inlet. The nozzle deflects the fluid jet by an angle $\theta$ and conveys the same amount of fluid as the tubes. Summing up, the total mass attached to the downstream end of the beam structure is $M = M_c + M_n$.

Assuming atmospheric pressure at the beam end, the small amplitude motion of the beam deflection $w(z, t)$ around the trivial equilibrium configuration is governed by the linear partial differential equation (Paidoussis & Li 1993)

$$m_l\ddot{w} + (D^*\dot{w}'')'' + ch\dot{w} + 2m_f u\dot{w}' + (Dw'')'' + g\left\{m_l w' - \left(\int_z^l m_l \,\mathrm{d}z + M\right)w''\right\} + m_f u^2 w'' = 0, \tag{1}$$

where a dot denotes differentiation with respect to time $t$ and a prime denotes differentiation with respect to $z$. The total mass per unit length of the beam structure is $m_l(z) = m_b(z) + m_t + m_f$ and $g$ is the acceleration due to gravity. The total stiffness distribution is $D(z) = E_b I_b(z) + E_t I_t$, and $D^*(z) = E_b^* I_b(z) + E_t^* I_t$ determines the total amount of structural damping. The viscous damping is assumed proportional to the beam width, determined by the viscous damping coefficient $c$.

Assuming small nozzle deflections, and neglecting dynamic forces from the nozzle motion and rotary inertia and viscous damping of the control system, the boundary conditions of the cantilevered configuration at $z = 0$ are simply

$$w = w' = 0, \tag{2}$$

while the boundary conditions defining the transverse force and bending moment at $z = l$ are

$$\begin{aligned}
&(Dw'')' + (D^*\dot{w}'')' + (M_c + M_n)\ddot{w} + \{M_c a_c + M_n(l_c + a_n)\}\ddot{w}' \\
&\quad + 2u(M_{fc} + M_{fn})\dot{w}' + g(M_c + M_n)w' + m_f u^2\theta = 0, \\
&Dw'' + D^*\dot{w}'' + \{M_c a_c + M_n(l_c + a_n)\}\ddot{w} + \{M_c a_c^2 + M_n(l_c + a_n)^2\}\ddot{w}' \\
&\quad + 2u\{M_{fc}a_{fc} + M_{fn}(l_c + a_{fn})\}\dot{w}' + g\{M_c a_c + M_n(l_c + a_n)\}w' \\
&\quad + gM_n a_n\theta + m_f u^2 l_c\theta = 0.
\end{aligned} \tag{3}$$

This result is derived in the appendix using a distributed mass approach based on the plug-flow approximation (Paidoussis & Li 1993) of the fluid-dynamic forces involved.

### 2.2. Numerical Analysis

Using a symmetric and piecewise linear beam width, the equation of motion (1) with boundary conditions (2) and (3) is discretized using Hermitian finite elements (Langthjem 1996). Denoting the nodal displacement vector $\mathbf{w}$, the discretized equations of motion may be written as

$$\mathbf{M}\ddot{\mathbf{w}} + (\mathbf{D} + u\mathbf{G})\dot{\mathbf{w}} + \mathbf{K}\mathbf{w} - u^2\mathbf{Q}\mathbf{w} = (\mathbf{p} + u^2\mathbf{q})\theta, \tag{4}$$

where

$$\begin{aligned} \mathbf{D} &= \delta_b\mathbf{K}_b + \delta_t\mathbf{K}_t + c_b\mathbf{M}_b, \\ \mathbf{K} &= \mathbf{K}_b + \mathbf{K}_t + \mathbf{K}_g, \\ \mathbf{Q} &= \mathbf{Q}_c - \mathbf{Q}_n, \end{aligned} \tag{5}$$

and the parameters $\delta_t = E_t^*/E_t$, $\delta_b = E_b^*/E_b$ and $c_b = c/\rho_b d$ have been introduced for convenience. The total mass matrix $\mathbf{M}$, the beam mass matrix $\mathbf{M}_b$, the beam and tube stiffness matrices $\mathbf{K}_b$ and $\mathbf{K}_t$, the gravity matrix $\mathbf{K}_g$ and the conservative load matrix $\mathbf{Q}_c$ are all symmetric and positive definite, while the Coriolis (gyroscopic) matrix $\mathbf{G}$ and the nonconservative load matrix $\mathbf{Q}_n$ are nonsymmetric. The force vector $\mathbf{p}$ corresponds to the gravity moment induced by the nozzle deflection, and $\mathbf{q}$ is the force vector corresponding to the force and moment due to the deflection of the fluid jet.

Introducing the state vector $\mathbf{z}$, the system matrix $\mathbf{A}$ and the input vector $\mathbf{b}$ according to

$$\mathbf{z} = \begin{Bmatrix} \mathbf{w} \\ \dot{\mathbf{w}} \end{Bmatrix}, \quad \mathbf{A} = \begin{bmatrix} \mathbf{0} & \mathbf{I} \\ > \mathbf{M}^{-1}(\mathbf{K} - u^2\mathbf{Q}) & -\mathbf{M}^{-1}(\mathbf{D} + u\mathbf{G}) \end{bmatrix}, \quad \mathbf{b} = \begin{Bmatrix} \mathbf{0} \\ \mathbf{M}^{-1}(\mathbf{p} + u^2\mathbf{q}) \end{Bmatrix}, \tag{6}$$

the discretized equations of motion (4) may be written in the state-variable form

$$\dot{\mathbf{z}} = \mathbf{A}\mathbf{z} + \mathbf{b}\theta. \tag{7}$$

The dynamics of an actuator may be included by merging equation (7) with a state-variable model of the actuator. This results in a new system in the same form but now the actuator set-point $\tilde{\theta}(t)$ is the control variable. A standard actuator model to be used further on, is given by the second-order model

$$\ddot{\theta} + 2\sigma\omega_0\dot{\theta} + \omega_0^2\theta = \omega_0^2\tilde{\theta}, \tag{8}$$

which is easily rewritten in state-variable form. Essentially, $\omega_0$ and $\sigma$ determine the speed and damping of the servo response, respectively. Note that the system given by (6) corresponds to the special case of an ideal actuator model $\theta(t) = \tilde{\theta}(t)$.

In this study, a simple output feedback control law (Stevens & Lewis 1992) is used to improve the stability of the system. Given some measured outputs defined by $\mathbf{y} = \mathbf{C}\mathbf{z}$, $\mathbf{C}$ being the output matrix, the control law is defined as the (positive) output feedback

$$\tilde{\theta} = \mathbf{k}^{\mathrm{T}}\mathbf{y} = \mathbf{k}^{\mathrm{T}}\mathbf{C}\mathbf{z}, \tag{9}$$

where $\mathbf{k}$ is a vector of feedback gains. Including the actuator dynamics, this control law yields the closed-loop system

$$\dot{\mathbf{z}} = \mathbf{A}\mathbf{z} + \mathbf{b}\tilde{\theta} = (\mathbf{A} + \mathbf{b}\mathbf{k}^{\mathrm{T}}\mathbf{C})\mathbf{z} = \tilde{\mathbf{A}}\mathbf{z}, \tag{10}$$

where $\tilde{\mathbf{A}} = \mathbf{A} + \mathbf{b}\mathbf{k}^{\mathrm{T}}\mathbf{C}$ is the closed-loop system matrix. Solutions of equation (10) are assumed to be on the form

$$\mathbf{z}(t) = \tilde{\mathbf{z}}\mathrm{e}^{\lambda t}, \tag{11}$$

which inserted in equation (10) gives the linear eigenvalue problem

$$(\tilde{\mathbf{A}} - \lambda\mathbf{I})\tilde{\mathbf{z}} = \mathbf{0}. \tag{12}$$

The structure is considered stable for a given flow speed if all eigenvalues $\lambda$ have negative real part. Further, the imaginary part of the eigenvalues is the (circular) frequency of vibration of the corresponding eigenmode.

## 3. EXPERIMENTAL APPROACH

For a description of the experimental set-up generating the water flow, the reader is referred to Borglund (1998). Essentially, the experimental procedures described in Borglund (1998) were used with only minor modifications. This paper emphasizes the control system set-up, schematically shown in Figure 2.

The nozzles are individually controlled by a personal computer (PC) using two high-performance linear electric servos. The displacement of the beam tip, directly corresponding to a state in the theoretical model, is measured by a triangulating optical (laser) displacement sensor. The sensor measures the distance to an object with a specified resolution of 60 μm within the range $\pm 100$ mm. The analog signal from the optical sensor is sampled by a PC with a data acquisition (DAQ) board.

The output feedback control law was written in the LabVIEW software (Johnson 1994), which enabled real-time adjustment of the feedback gain. Controlling the two servos in parallel, the system provided a control-loop frequency of approximately 143 Hz. In the theoretical analysis the system is considered time-continuous.

### 3.1. Structural Design and Material Parameters

The same structural design as described in Borglund (1998) was used with only a few modifications. In the present study composite beams of two different nominal thicknesses $d_0$ were used. The glass/epoxy composite provided much higher accuracy in the thickness distribution than the material used in Borglund (1998). The elastic properties of the composite material were determined using a dynamic technique (Kuttenkeuler 1998). As in the previous study (Borglund 1998), reinforced silicone rubber tubes with inner and outer diameter 8·0 and 14·0 mm were used. The properties of the two different laminate-tube configurations are given in Table 1.

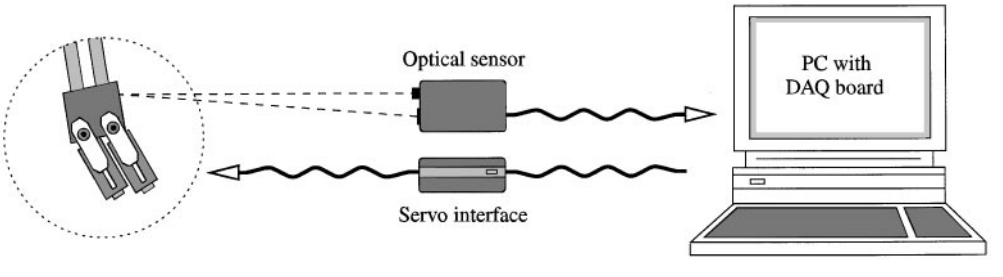


Figure 2. Schematic layout of the control system set-up.

TABLE 1

Properties of the beam-tube configurations

| Property | Config. 1 | Config. 2 | Units |
|---|---|---|---|
| $d_0$ | 0·0010 | 0·0015 | m |
| $\rho_b$ | 1927 | 1900 | kg/m$^3$ |
| $\rho_t$ | 1225 | 1225 | kg/m$^3$ |
| $E_b$ | $21{\cdot}49 \times 10^9$ | $23{\cdot}08 \times 10^9$ | N/m$^2$ |
| $E_t$ | $5{\cdot}43 \times 10^6$ | $5{\cdot}43 \times 10^6$ | N/m$^2$ |
| $E_b^*$ | $7{\cdot}22 \times 10^7$ | $2{\cdot}37 \times 10^7$ | N s/m$^2$ |
| $E_t^*$ | $7{\cdot}87 \times 10^5$ | $7{\cdot}10 \times 10^5$ | N s/m$^2$ |
| $c$ | 0·114 | 0·114 | kg/m$^2$s |

TABLE 2

Properties of the nozzle control system

| Property | Value | Units |
|---|---|---|
| $M_c$ | 0·2690 | kg |
| $M_n$ | 0·0534 | kg |
| $M_{fc}$ | 0·0025 | kg |
| $M_{fn}$ | 0·0035 | kg |
| $l_c$ | 0·0250 | m |
| $l_n$ | 0·0350 | m |
| $a_c$ | 0·0065 | m |
| $a_n$ | 0·0187 | m |

The viscoelastic properties of the materials were determined as described in Borglund (1998) with the only difference that the optical sensor was used in the vibration tests. This made vibration tests with very small amplitudes possible, hence the somewhat different values of the damping parameters compared with the values given in Borglund (1998). The density of the water was assumed to be $\rho_f = 1000$ kg/m$^3$ and the acceleration due to gravity $g = 9{\cdot}81$ m/s$^2$.

The nozzle control mechanism was manufactured in aluminium. The main part of the nozzles is a short aluminium pipe, bending the tube going through the nozzle control system, see Figure 1. In the theoretical model, the fluid jet is assumed to be abruptly deflected at the axis of rotation of the nozzle. Consequently, this axis defines the theoretical position of the nozzle inlet. The servo control wires, not included in the theoretical model, were drawn along the tubes. The experimentally determined properties of the nozzle control system is given in Table 2.

### 3.2. CONTROL SYSTEM VALIDATION

After a static calibration of the servo-nozzle mechanism, the parameters in the actuator model, equation (8), were determined by a least-squares fit to experimental data for a step response of magnitude $\Delta\tilde{\theta} = 0{\cdot}01$ rad. The values $\sigma = 0{\cdot}763$ and $\omega_0 = 173{\cdot}5\,\mathrm{s}^{-1}$ were obtained. The nozzle control system was attached to a uniform beam structure with length $l = 1{\cdot}045$ m, constant width $h = 0{\cdot}15$ m and average thickness $d = 1{\cdot}05$ mm, with properties according to Configuration 1 in Table 1. The static force from a deflection of the fluid jets

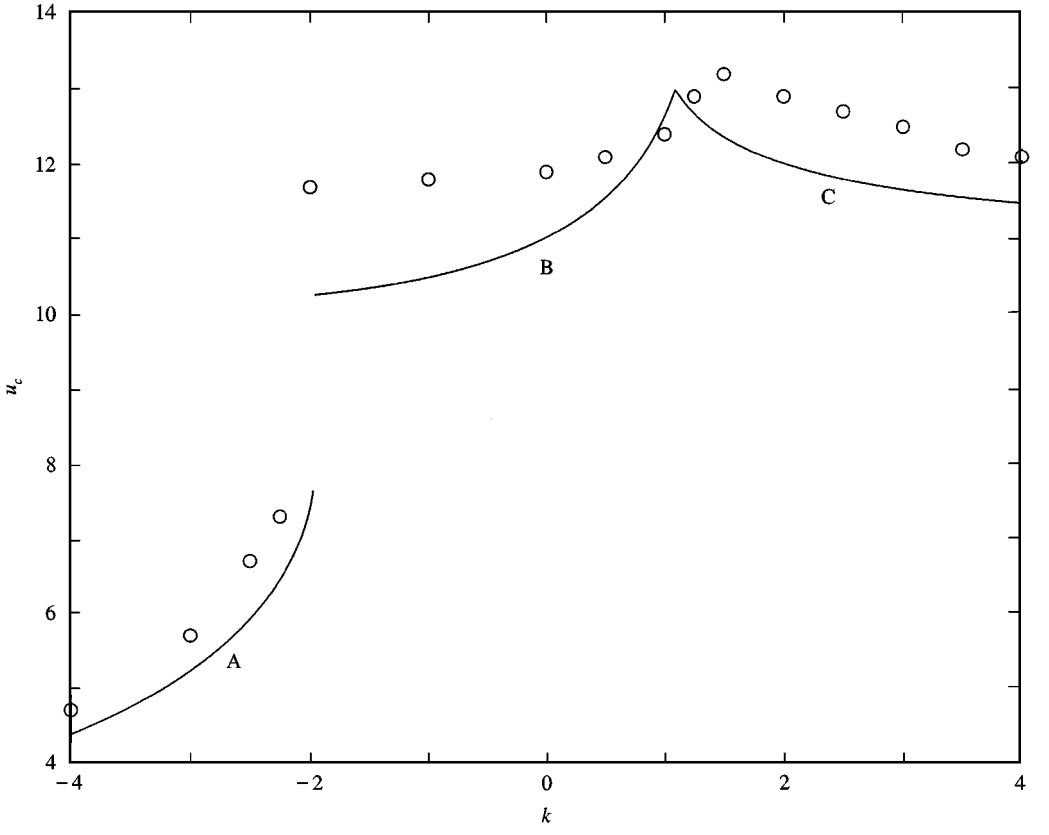


Figure 3. Critical speed versus feedback gain for the uniform beam.

was measured using an electronic force-gauge. For deflections ranging up to 0·2 rad, the average deviation between the measurements and the theoretical prediction $F = m_f u^2 \tilde{\theta}$ was only 3%. Thus, no correction in the model was made.

The control law used in the experiment is given by

$$\tilde{\theta} = ky, \tag{13}$$

where $y(t)$ is the displacement of the beam tip and $k$ the constant feedback gain. Besides being easily implemented in the experiment, the simplicity of this control law enables close investigation of the impact of the control system on the stability and optimal design. The theoretical prediction of the critical speed $u_c$ (m/s) for various feedback gain $k$ (rad/m) is shown by the solid line in Figure 3. The numerical analysis was carried out with 16 finite elements.

Depending on the feedback gain, three different instability modes are possible, denoted A, B and C in the figure. For the case without control ($k = 0$), the usual flutter mode (B) is critical. If the feedback gain is reduced, the critical speed eventually falls discontinuously when the mode transition from B to A takes place. Mode A is a divergence mode with a shape similar to Euler's first buckling mode (clamped-free boundary conditions). For increasing $k > 0$ the critical speed eventually reaches a maximum, where a transition to mode C occurs. Mode C corresponds to another divergence mode with a shape resembling Euler's third buckling mode (clamped-hinged boundary conditions). The

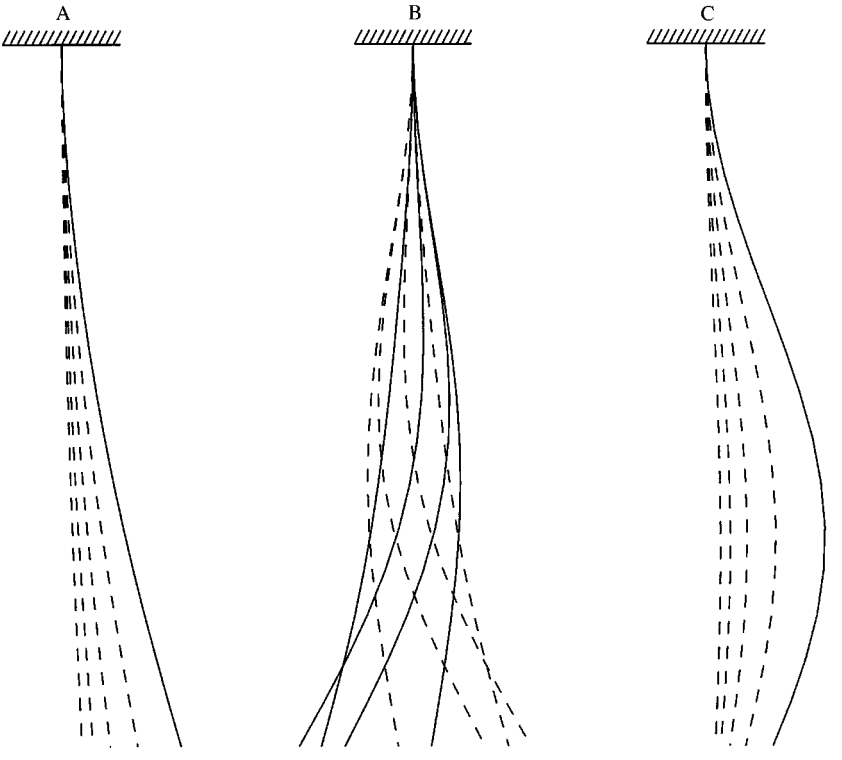


Figure 4. Illustration of the different instability modes.

different instability modes are illustrated in Figure 4. In the illustration of the flutter mode B, the solid lines correspond to rightward motion of the beam tip and the dashed lines correspond to leftward motion.

Consequently, the maximum stabilizing effect is achieved at a feedback gain where a transition from flutter to divergence occurs. This is in accordance with results in Sugiyama *et al.* (1985), where it is concluded that the most stabilizing effect due to a spring support may be obtained by finding the critical spring constant at which the transition of the instability mechanism from flutter to divergence takes place.

Using the experimental methodology described in Borglund (1998), the critical speed was experimentally determined for a set of different feedback gains, marked by dots in the graph of Figure 3. The predicted instability modes were clearly observed. The critical speeds of the divergence modes were easily determined due to a rather distinct divergence behaviour, while the flutter mode was more difficult. Without control, flutter was initiated at the critical speed of 11·9 m/s. The theoretical prediction is 11·0 m/s, giving an error of 8%. The flutter frequency was 1·6 Hz in the experiment and 1·4 Hz theoretically, a 13% error. For $k < 0$ the flutter instability was distinct and extremely violent, which was not the case for $k \geq 0$. This indicates a transition from a supercritical to a subcritical Hopf bifurcation (Langthjem 1996) at $k = 0$ due to the reversed control action.

For $k > 0$, small limit-cycle motion was observed for subcritical speeds higher than the critical speed at $k = 0$. There are two probable reasons for this. First, a small play in the nozzle mechanism was observed during the calibration process. The second reason is the sampling dead-time in the control system. Both may result in a loss of asymptotic stability in an inherently unstable system. It may be possible to analyse the effect of a lag in the

control system on the stability, but this is considered to be beyond the scope of the present paper. In obtaining the values of the critical speed presented in Figure 3, the limit-cycle motion was not considered as an instability. It was still possible to approximately determine the speed where flutter developed. The experimental maximum of the critical speed was characterized by flutter breaking into divergence. Neglecting the limit-cycle motion, the predicted instability modes were observed with an average error in the critical speed of 7% (excluding the point at the discontinuity). However, if the control system is to be used for design purposes, a more accurate prediction of the most stabilizing gain would be desirable.

The most likely reason for the observed offset between the theoretical and experimental peaks in Figure 3 is a lag in the control system, i.e., an offset between the set-point for and the predicted nozzle deflection. Among other sources, such as the sampling dead-time, the small play in the nozzle mechanism was found to be dominating. The low value of the optimal feedback gain means that the system is very sensitive to supporting forces at the beam tip, which was also concluded in Sugiyama *et al.* (1985). This leads to small nozzle deflections, which means that even a small play in the nozzle mechanism may have a large impact on the dynamics. For a feedback gain $k \approx 1$ rad/m and a beam tip displacement $y \approx 0{\cdot}01$ m, a $0{\cdot}003$ rad play in the nozzle mechanism may result in a 30% deflection lag. The given orders correspond to the optimal feedback gain, the amplitude of the limit cycle and the observed play in the nozzle mechanism. Obviously, the control system is prone to uncertainties that are difficult to include in the model. However, one may interpret the characteristics in Figure 3 as being caused by an uncertainty in the feedback gain. This is discussed further in Section 4.3.

## 4. OPTIMAL DESIGN

It is well known that the critical load of structures subject to nonconservative forces may be a nonsmooth, possibly discontinuous, function of the design (Langthjem 1996; Kuttenkeuler & Ringertz 1998a). By considering the feedback gain as a design variable, it is obvious from Figure 3 that this holds for the present system. This means that the optimization problem of maximizing the critical flow speed for a fixed amount of structural mass (or volume) would not be well posed. Instead, the formulation of minimizing structural mass at fixed critical flow speed is preferable, since the structural mass is a well-behaved function of the design.

The problem of minimizing the beam structural mass $m$ for a specified critical flow speed $u_c$ is posed as the nonlinear programming problem

$$\min_{x_j} m(x_j) \tag{14}$$

$$\mathscr{R}e\,\lambda_i(x_j, u) \leq 0, \quad i = 1 \ldots n_\lambda, \quad u \in [0, u_c], \tag{15}$$

$$x_j \geq \underline{x}_j, \quad j = 1 \ldots n_x, \tag{16}$$

where $\lambda_i$ are the eigenvalues obtained by solving the eigenvalue problem (12) and $x_j$ the design variables. In the present work, beam nodal widths and feedback gains in the control law (9) are the possible design variables.

It should be noted that the optimization problem defined by equations (14)–(16) is still nonsmooth. The eigenvalues (and hence the stability constraint functions (15)) are continuous functions of the design variables, but may be nonsmooth when there are coalescing eigenvalues (Seyranian 1993). However, if the eigenvalues are distinct at the solution, the

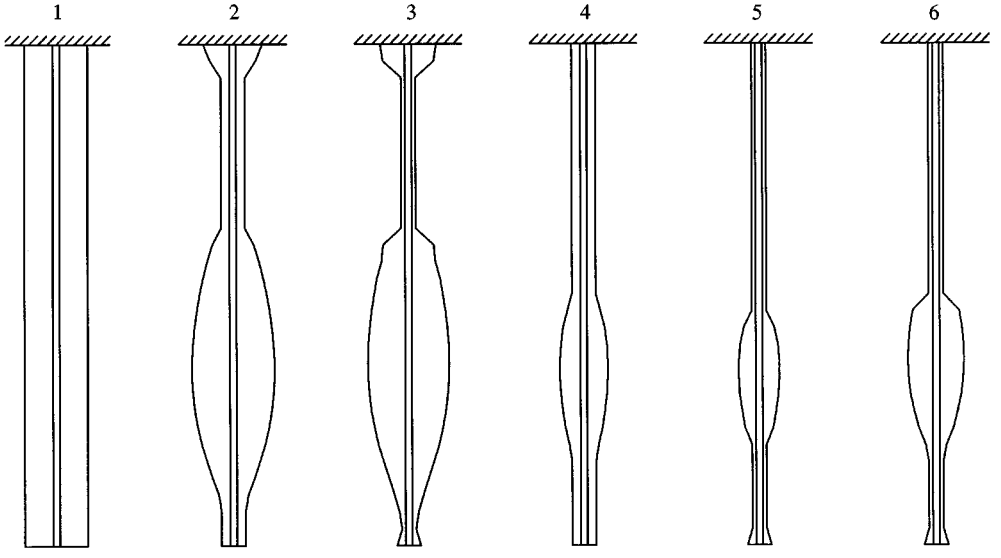


Figure 5. Investigated beams; the numbers on top refer to "Design 1", "Design 2", *et sec.*

problem may usually be solved using standard numerical optimization techniques. In this study, the problem is solved using the method of moving asymptotes (MMA) developed by Svanberg (1993). The derivatives of the constraint functions (15) exist provided that the eigenvalues of equation (12) are distinct, and are derived as described in Haftka & Adelman (1993).

### 4.1. Optimal Design without Control Action

In the following, all beams considered have the properties according to Configuration 2 in Table 1, and were manufactured from the same composite laminate in the experiment. The reference for the design improvements is a uniform beam with length $l = 1{\cdot}045$ m, width $h_0 = 0{\cdot}13$ m and average thickness $d = 1{\cdot}52$ mm, shown as Design 1 in Figure 5.

The first optimal design problem considered is to find the beam width distribution, such that the beam structural mass is minimized for the specified critical flow speed $u_c = 14{\cdot}2$ m/s, which is the predicted critical speed of the uniform design. Note that the nozzle control system is physically present but disabled ($k = 0$). This problem was treated in detail in Borglund (1998) and the results are summarized as follows. The beam geometry is divided into 30 finite elements of equal length and linearly varying width, giving 31 beam nodal widths representing the design variables. The initial values $h_j = h_0$ were used, and the stability constraints were only enforced for the flow speed $u = 14{\cdot}2$ m/s. Using two different sets of lower bounds on the beam width $\underline{h}_j = 0{\cdot}05$ m and $\underline{h}_j = 0{\cdot}03$ m, the optimal design shown as Design 2 and 3 in Figure 5 are obtained. To simplify the attachment of the control system, the minimum width of the beam tip is 0·05 m in both cases. The optimization problem was solved in approximately 30 iterations, giving a maximum residual in the design variables of less than $10^{-4}$ (m).

The theoretical results are compared with experiments in Table 3. The ratio between the beam structural mass of the optimal design and the reference design is used as a measure of the design improvements. Note that the optimization problems were solved using different beam thicknesses, measured in the experiment. Good agreement between numerical

TABLE 3

Properties of the investigated beams and comparison with experiments

| Design | $d$ (mm) | $\frac{h}{m}$ | Mass ratio (%) | $k^*$ (rad/m) | $u_{pred}$ (m/s) | $u_{exp}$ (m/s) | Error (%) |
|---|---|---|---|---|---|---|---|
| 1 | 1·52 | — | 100 | — | 14·2 | 14·4 | 1·4 |
| 2 | 1·54 | 0·05 | 76 | — | 14·2 | 14·4 | 1·4 |
| 3 | 1·55 | 0·03 | 71 | — | 14·2 | 14·7 | 3·5 |
| 4 | 1·55 | 0·05 | 48 | 1·28 | 14·2 | 13·0 | 8·8 |
| 5 | 1·53 | 0·03 | 31 | 1·23 | 14·5 | 12·5 | 15 |
| 6 | 1·55 | 0·03 | 39 | 1·45 | 14·9 | $> 15·0$ | — |

predictions and experiments were achieved. All of the investigated beams (1–3) became unstable in the flutter mode B described in Section 3.2, which was also predicted. The deviation between the theoretical and the experimental flutter frequency was less than 10% in all cases.

### 4.2. INTEGRATED OPTIMAL DESIGN

The problem stated in this section is to find both the beam width *and* the feedback gain in the control law (13), such that the beam structural mass is minimized for the critical flow speed $u_c = 14·2$ m/s.

The same discretization, initial values and lower bounds on the beam nodal widths as in the previous section were used. The initial value $k = 0$ was chosen for the feedback gain, corresponding to an initially disabled control. No bounds were put on the gain. Solving the optimal design problem with the same termination criteria for the iterations, Designs 4 and 5 in Figure 5 are obtained. To ensure stability of Design 5 for $u \in [0, u_c]$, the stability constraints were enforced for the set $u = \{12·5, 12·6, \ldots, 14·2\}$ m/s. The results from the optimization are given in Table 3. The optimal feedback gain is denoted $k^*$.

The inclusion of the control system in the optimization gives a significant reduction of the beam structural mass. Design 5 has a total beam mass reduction of 69%! However, the optimal beams were both experimentally unfeasible. If the optimal feedback gain were used in the experiment, both Design 4 and 5 became unstable in flutter at a lower speed than the specified 14·2 m/s. The reasons for this is explained in the following.

In Figure 6 the critical speed for varying feedback gain is shown for Design 4 in the same manner as in Section 3.2. A more thorough experimental investigation reveals that the lag in the control system is the reason for the unfeasibility. This is clearly observed in Figure 6, where the experiment corresponding to the optimal feedback gain is marked by "∇". The optimal design is characterized by a multiple bifurcation where the flutter mode B and the divergence mode C becomes critical simultaneously. This is visualized in Figure 7 by plotting the real part of the relevant eigenvalues (the relevant stability constraint functions) versus the flow speed for the optimal feedback gain. The flutter mode B is readily followed to instability at $u = 14·2$ m/s. The divergence mode C appears when the complex conjugate eigenvalues corresponding to a flutter mode coalesce and form a new pair of real eigenvalues. This is known as strong interaction between two eigenvalues (Seyranian 1993). For beams 1–3, without control action, no interaction occurs before the flutter mode B becomes unstable. Finally, modes B and C become critical simultaneously at the specified critical speed, marked by "o" in the figure. Note that the critical eigenvalues are still distinct, since they are separated in frequency.

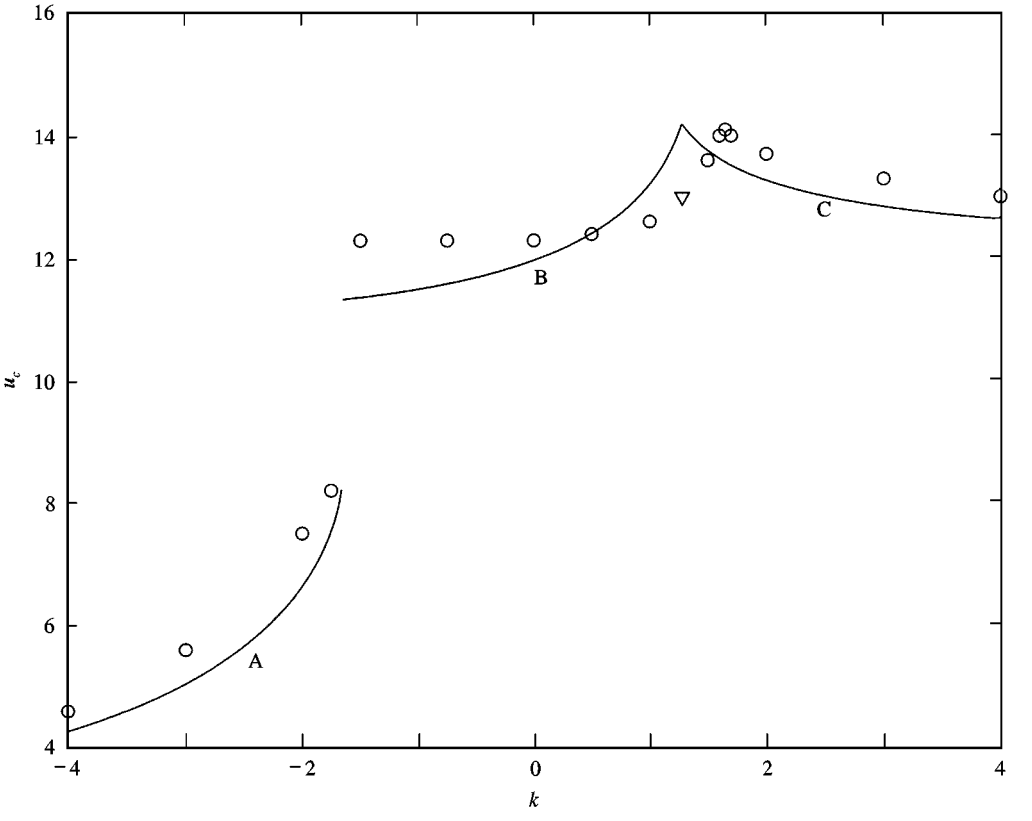


Figure 6. Critical speed versus feedback gain for Design 4.

The behaviour of Design 5 is more complicated. The corresponding plots are shown in Figures 8 and 9. In Figure 9 it is observed that mode C is critical at $u \approx 12{\cdot}8$ m/s but is stabilized again for increasing $u$. The same thing happens for mode B at $u \approx 13{\cdot}6$ m/s. In between these speeds, the two real eigenvalues coincide and a flutter mode reappears (mode D in the figure). Instability does not occur until this mode becomes critical at $u = 14{\cdot}5$ m/s. This means that none of the stability constraints are active at the specified critical speed 14·2 m/s (marked by "o" as before), which is certainly an interesting feature of this design.

The scenario described above explains the characteristics in Figure 8. At $k = k^*$ instability occurs at 14·5 m/s in mode D, marked by '$*$' in the plot. If the feedback gain is perturbed according to $k = k^* + \Delta k$, $\Delta k > 0$, the critical speed drops discontinuously to 12·8 m/s due to a transition to the divergence mode C. In the same manner, a perturbation $k = k^* - \Delta k$ results in a transition to the flutter mode B, and the critical speed drops to 13·6 m/s. Consequently, the optimal design is extremely sensitive to uncertainty in the feedback gain. Imperfections in the structural design will have the same effect.

With the above findings in mind, the poor performance of Design 5 in the experiment is not surprising. A small lag in the control system results in a severe drop in critical speed due to the sensitivity of the optimal design. Somewhat surprisingly though, it was possible to find a feedback gain in the experiment where it was difficult to distinguish between the predicted instability modes and the limit-cycle motion described in Section 3.2. At this gain it was possible to increase the flow speed to 15 m/s, which was the maximum speed provided by the experimental set-up. This speed is marked by "$\diamond$" in Figure 8 and does not

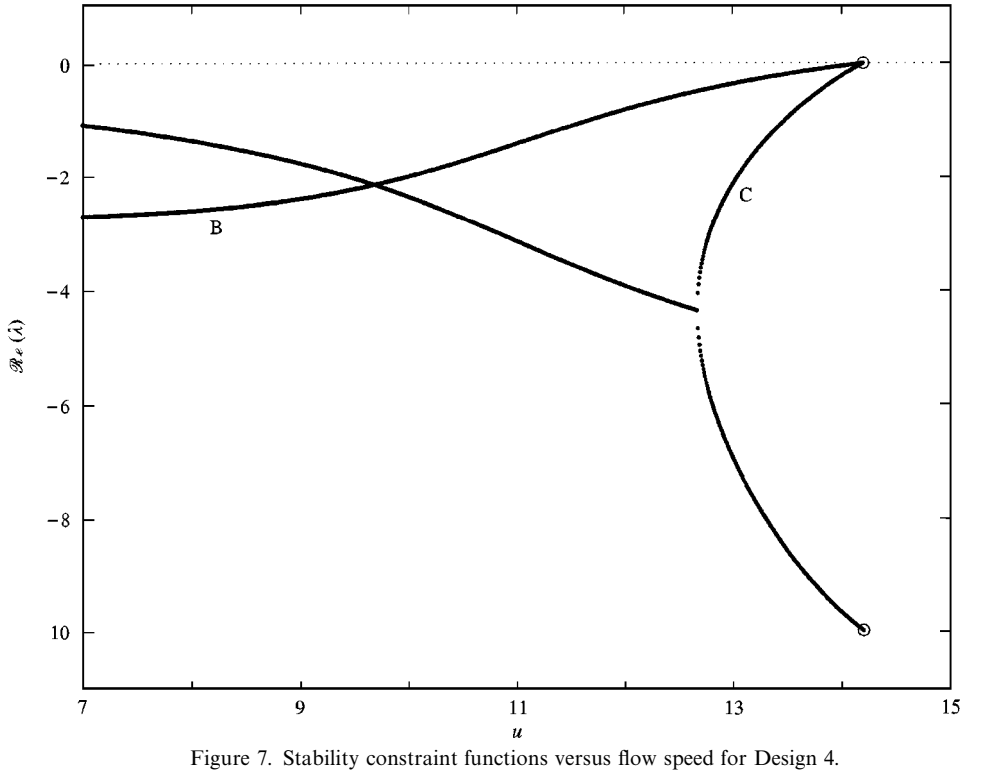


Figure 7. Stability constraint functions versus flow speed for Design 4.

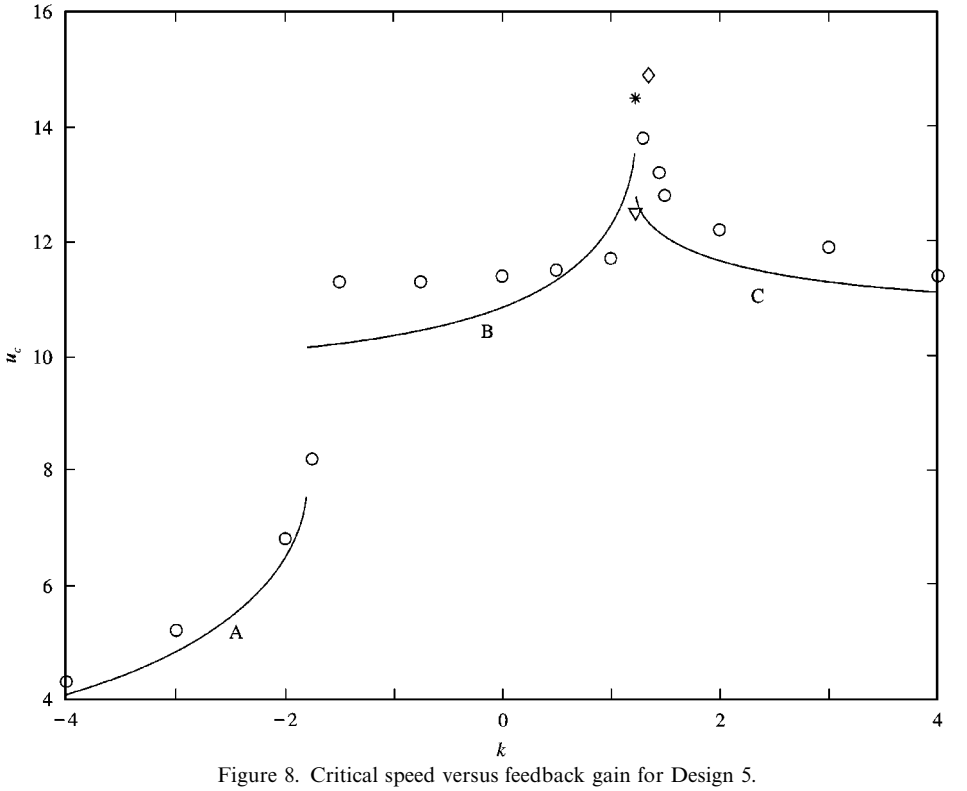


Figure 8. Critical speed versus feedback gain for Design 5.

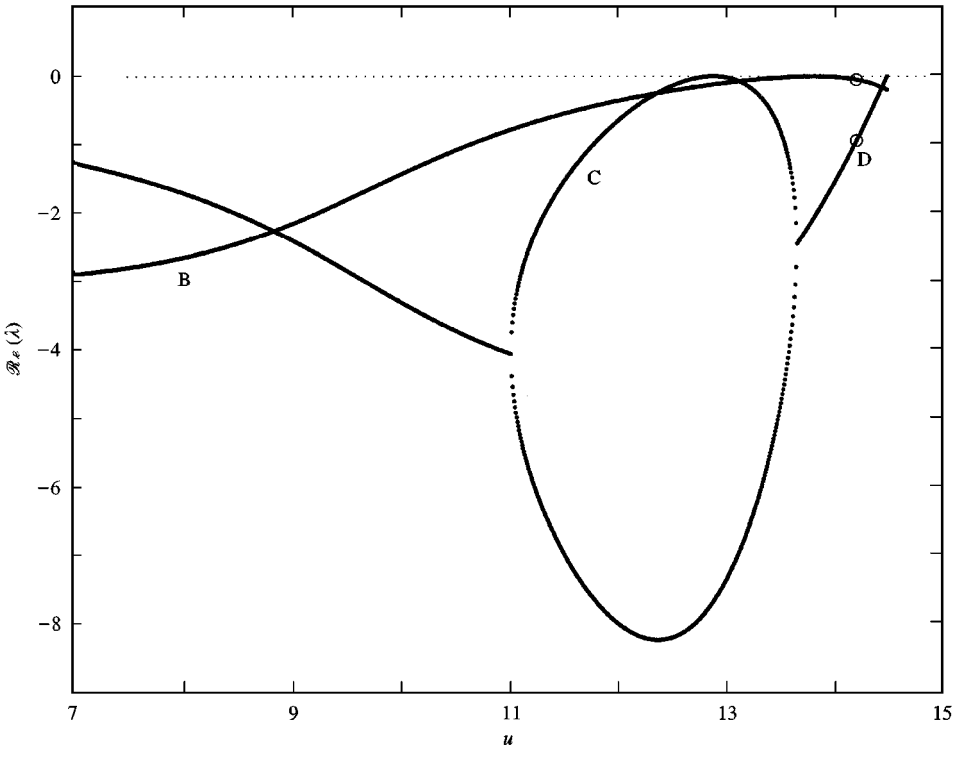


Figure 9. Stability constraint functions versus flow speed for Design 5.

correspond to instability. At this speed the structure was very well behaved, and strong perturbations were damped out within a few cycles. This verifies that modes B and C are stabilized as predicted. If the control system was shut off, the structure responded like a whiplash.

If the ideal actuator model $\theta(t) = \tilde{\theta}(t)$ is used in the prediction of the critical speed, mode D becomes critical on a finite interval of width $\Delta k \approx 0{\cdot}1$ rad/m due to the increased actuator efficiency. This indicates that the actuator dynamics has impact on the design, and also implies that an experimentally unfeasible design may result if the ideal model is used in the optimization.

### 4.3. Integrated Optimal Design Considering Control Uncertainty

As mentioned at the end of Section 3.2, one may interpret the lag characteristics in Figures 3, 6 and 8 as being caused by an uncertainty in the feedback gain corresponding to a systematic use of too low a gain in the experiment. In the following, this is assumed to be the only uncertainty in the system, which is a reasonable assumption considering the results for the case without control (see Section 4.1). One would thus like to obtain an optimal design persistent to perturbations of the kind $k = k^* - \Delta k$, where $\Delta k \geq 0$ is a (possibly large) prescribed uncertainty in the feedback gain.

It is realized that if the flutter mode B in Figures 7 and 9 would have a margin to instability for all speeds $u \in [0, u_c]$, the structure would be stable for some interval $[k^* - \Delta k, k^*]$ of the feedback gain. This means that a design with the desired property may be obtained by enforcing a stability margin on mode B in the optimization. More generally,

this modified optimization problem may be written in the form

$$\min_{x_j} m(x_j) \tag{17}$$

$$\mathscr{R}e\,\lambda_i(x_j, u) + \delta_i \leq 0, \quad i = 1 \ldots n_\lambda, \quad u \in [0, u_c], \tag{18}$$

$$x_j \geq \underline{x}_j, \quad j = 1 \ldots n_x, \tag{19}$$

where $\delta_i$ is the stability margin corresponding to mode $i$. This formulation is used for example by Kuttenkeuler & Ringertz (1998b), where it is also noted that finding the proper stability margins is not a trivial task.

For this small problem though, where uncertainty in only one parameter is considered, a sufficient stability margin is found by inspection as follows. By enforcing a stability margin on mode B of $\delta = 0{\cdot}75\ \mathrm{s}^{-1}$ but otherwise using the problem formulation for Design 5, the optimal Design 6 in Figure 5 is obtained. The specified stability margin is readily verified in Figure 11. As for Design 5, none of the stability constraints are active at the specified critical speed 14·2 m/s, and instability (in mode D) does not occur until 14·9 m/s. In this case though, mode D is critical on a finite interval of the feedback gain, see Figure 10. By inspection, the structure is feasible for $k \in [k^* - \Delta k, k^*]$, where $\Delta k \approx 0{\cdot}4$ rad/m covers the peak offsets observed in Figures 6 and 8. Hence, the modified design is expected to be experimentally feasible. As shown in Figure 10, the structure was found to be well behaved (see Section 4.2) for the optimal feedback gain. Further, this behaviour was observed for

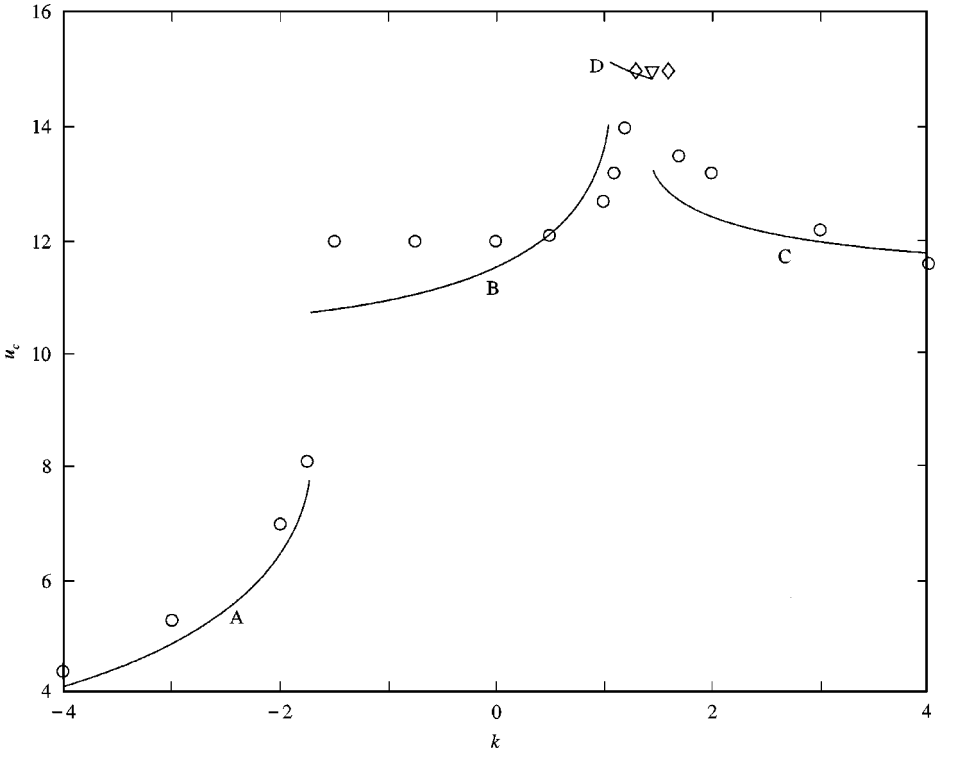


Figure 10. Critical speed versus feedback gain for Design 6.

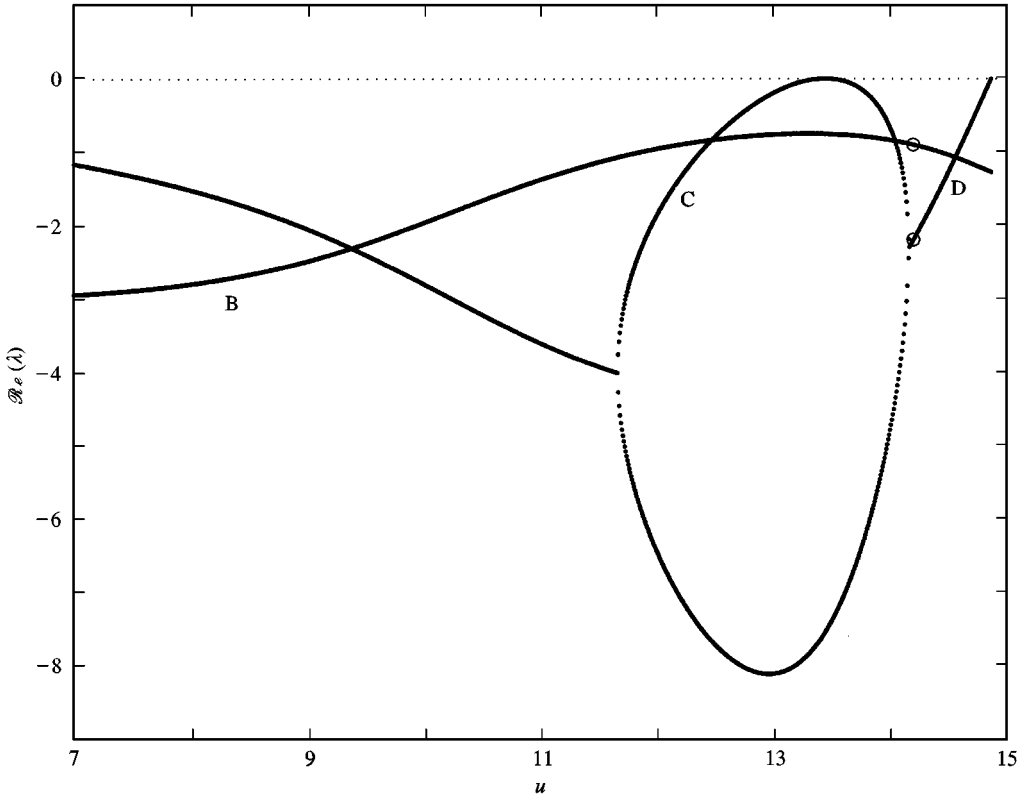


Figure 11. Stability constraint functions versus flow speed for Design 6.

a finite interval of the feedback gain of approximately the predicted width. Unfortunately, the flow speed could not be increased high enough to verify the predicted flutter instability (mode D).

As presented in Table 3, the robust optimal design still has 61% less structural mass than the reference design. Hence, at the cost of a moderate increase in structural mass, a robust design with significantly improved performance is obtained by enforcing a stability margin in the optimization.

## 5. CONCLUSIONS AND DISCUSSION

Linear pipe-flow theory was found very capable of predicting the effect of active nozzle control on the stability of a flexible beam-tube structure. A simple proportional feedback gave rise to instability modes not present in the uncontrolled system, and the greatest stabilizing effect was achieved for a feedback gain at which a transition from flutter to divergence took place.

The inclusion of the control system in the design optimization gave a significant reduction of the beam structural mass and also introduced a new instability mode. The new flutter mode enabled an optimal design with the interesting feature of being damped at the minimum critical speed specified in the optimization. However, the integrated optimal design was found to be very sensitive to imperfections and, consequently, the predicted performance could not be experimentally verified.

The main uncertainty in the system was a lag in the control system caused by a small play in the nozzle mechanism. By interpreting the lag as an uncertainty in the feedback gain, it was possible to obtain an experimentally feasible design by solving a modified optimization problem. The robust optimal design had approximately half the mass of an optimal design without control. In addition, it had a superior behaviour at the specified minimum critical speed, where it showed a significant persistence to strong perturbations. As stated in Kuttenkeuler & Ringertz (1998b), the modified formulation (17)–(19) is by no means the best way to achieve a robust optimal design, but the usefulness of an optimization formulation taking uncertainties into account was clearly demonstrated.

The present study has shown that significant improvements is possible using integrated design optimization. However, to achieve a performance that can be realized in practice, care must be taken in formulating the optimization problem. It would of course be possible to further increase the performance using a more advanced control law. However, such an improvement would most likely introduce additional uncertainties, which further necessitates the use of a robust optimization. Nevertheless, the present study has shown that by use of optimization techniques, even the simplest control system may have good performance.

## ACKNOWLEDGEMENTS

The author would like to thank his supervisor Professor Ulf Ringertz for much insightful advice and numerous rewarding discussions. He also acknowledge Dr Jakob Kuttenkeuler for experimental support and thorough comments on the paper. The project was financially supported by the Swedish Research Council for Engineering Sciences (TFR).

## References

Borglund, D. 1988 On the optimal design of pipes conveying fluid. *Journal of Fluids and Structures* **12,** 353–365.

Chen, S. S. & Jendrzejczyk, J. A. 1985 General characteristics, transition, and control of instability of pipes conveying fluid. *Journal of the Acoustical Society of America* **77,** 887–895.

Haftka, R. T. & Adelman, H. M. 1993 Sensitivity of discrete systems. In *Optimization of Large Structural Systems*, (ed. G. I. N. Rozvany), vol. 1, pp. 289–311. Dortrecht: Kluwer.

Johnson, G. W. 1994 *LabVIEW Graphical Programming*. New York: McGraw-Hill.

Kuttenkeuler, J. 1998 A finite element based modal method for determination of plate stiffnesses considering uncertainties. *Journal of Composite Materials*, to appear.

Kuttenkeuler, J. & Ringertz, U. 1998a Aeroelastic design optimization with experimental verification. *AIAA Journal of Aircraft* **35,** 505–507.

Kuttenkeuler, J. & Ringertz, U. 1998b Aeroelastic tailoring considering uncertainties in material properties. *Structural Optimization* **15,** 157–162.

Langthjem, M. A. 1996 Dynamics, stability and optimal design of structures with fluid interaction. Ph.D. Thesis, DCAMM Report S 71, Department of Solid Mechanics, The Technical University of Denmark.

Païdoussis, M. P. & Li, G. X. 1993 Pipes conveying fluid: a model dynamical problem. *Journal of Fluids and Structures* **7,** 137–204.

Seyranian, A. P. 1993 Sensitivity analysis of multiple eigenvalues. *Mechanics of Structures and Machines* **21,** 261–284.

Stevens, B. L. & Lewis, F. L. 1992. *Aircraft Control and Simulation*. New York: Wiley.

Sugiyama, Y., Tanaka, Y., Kishi, T. & Kawagoe, H. 1985 Effect of a spring support on the stability of pipes conveying fluid. *Journal of Sound and Vibration* **100,** 257–270.

Svanberg, K. 1993 The method of moving asymptotes (MMA) with some extensions. In *Optimization of Large Structural Systems* (ed. G. I. N. Rozvany), Vol. 1 pp. 555–566. Dortrecht: Kluwer.

TANAKA, M., TANAKA, S. & SEGUCHI, Y. 1993 Optimal and robust shapes of a pipe conveying fluid. In *Proceedings of the Asia-Pacific Vibration Conference* '93 Vol. 4, pp. 1757–1762. JSME.

YAU, C. H., BAJAJ, A. K. & NWOKAH, O. D. I. 1995 Active control of chaotic vibration in a constrained flexible pipe conveying fluid. *Journal of Fluids and Structures* **9,** 99–122.

ZHOU, R. C., LAI, Z., XUE, D. Y., HUANG, J. K., & MEI, C. 1995 Suppression of nonlinear panel flutter with piezoelectric actuators using finite element method. *AIAA Journal* **33,** 1098–1105.

## APPENDIX: DERIVATION OF BOUNDARY CONDITIONS

The transverse force and bending moment applied to the beam tip is most simply derived by considering the nozzle control system as an extension of the beam-tube structure, modelled as two articulated rigid pipes as shown in Figure 12. Assuming small amplitude motion, this means that the force per unit length

$$f = m_l\ddot{w} + 2m_f u\dot{w}' + g\left(m_l w' - \int_z^{l+l_c+l_n} m_l \,\mathrm{d}z\; w''\right) + m_f u^2 w'' \tag{A1}$$

has to be applied to achieve a motion $w(z, t)$ of the pipes. As before, $m_l(z)$ is the total mass per unit length of the structure. Also note that the viscous damping force is neglected.

Using the local length coordinate $\xi = z - l$ and the geometry defined in the figure, the linear approximation of the displacement along the pipes is

$$w(z, t) = \begin{cases} w_l(t) + w_l'(t)\xi, & 0 \le \xi \le l_c, \\ w_l(t) + w_l'(t)\xi + \theta(t)(\xi - l_c), & l_c \le \xi \le l_c + l_n, \end{cases} \tag{A2}$$

where $w_l(t)$ and $w_l'(t)$ is the displacement and rotation of the beam at $z = l$. Inserting equation (A2) in equation (A1) and integrating for the total force $T_0 = \int_0^{l_c+l_n} f(\xi)\,\mathrm{d}\xi$ and moment $M_0 = \int_0^{l_c+l_n} f(\xi)\xi\,\mathrm{d}\xi$

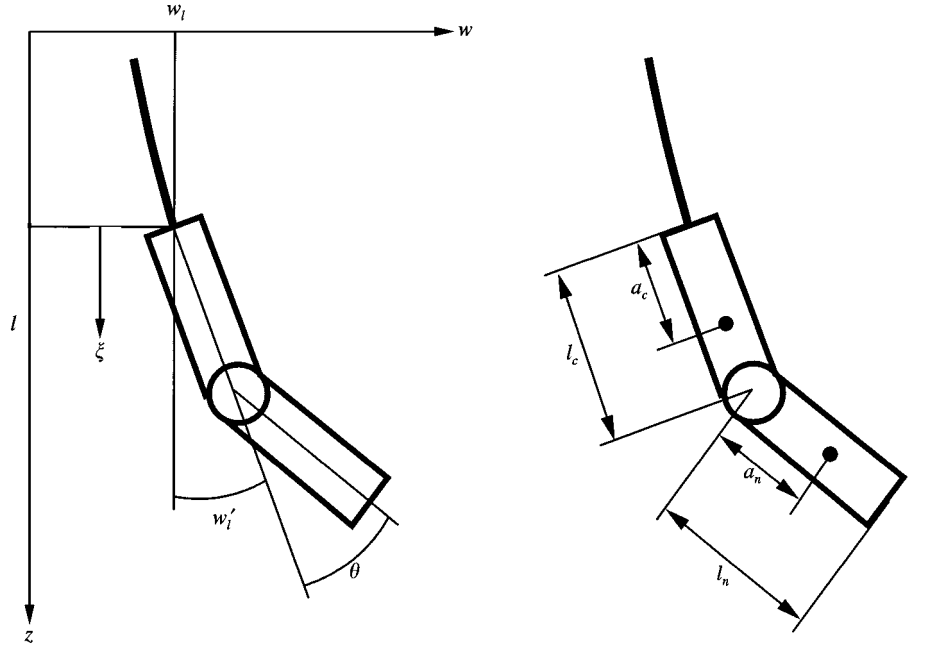


Figure 12. Schematic layout of the nozzle control system.

applied to the control system at $\xi = 0$ yields

$$\begin{aligned} T_0 &= (M_c + M_n)\ddot{w}_l + \{M_c a_c + M_n(l_c + a_n)\}\ddot{w}_l' + 2u(M_{fc} + M_{fn})\dot{w}_l' \\ &\quad + g(M_c + M_n)w_l' + M_n a_n\ddot{\theta} + 2uM_{fn}\dot{\theta} + m_f u^2\theta, \\ M_0 &= \{M_c a_c + M_n(l_c + a_n)\}\ddot{w}_l + \{(M_c a_c^2 + J_c) + (M_n(l_c + a_n)^2 + J_n)\}\ddot{w}_l' \\ &\quad + 2u\{M_{fc}a_{fc} + M_{fn}(l_c + a_{fn})\}\dot{w}_l' + g\{M_c a_c + M_n(l_c + a_n)\}w_l' \\ &\quad + \{M_n a_n(l_c + a_n) + J_n\}\ddot{\theta} + 2uM_{fn}(l_c + a_{fn})\dot{\theta} + gM_n a_n\theta + m_f u^2 l_c\theta, \end{aligned} \tag{A3}$$

with notation as defined in Section 2.1, except for the rotary inertia $J_c$ and $J_n$ of the control system and nozzle. Finally, a force and moment balance at $z = l$ give the boundary conditions for the beam-tube structure.

For the problem at hand, the dynamic forces proportional to $\dot{\theta}$ and $\ddot{\theta}$ are at least one order of magnitude smaller than the static force proportional to $\theta$, and are neglected. Further, rotary inertia of the control system and nozzle is neglected. Using these approximations, boundary conditions (3) are obtained.